Batteries & Supercaps

Research Article
doi.org/10.1002/batt.202200431

Chemistry Europe
European Chemical Societies Publishing

www.batteries-supercaps.org

Special Collection

High-Performance Aqueous Zinc-Organic Battery Achieved by Reasonable Molecular Design

Zhi Li[+],[a] Yu Zhang[+],[a] Jie Xu,[a] and Yonggang Wang*[a]

Aqueous zinc-organic batteries are considered as a promising candidate for the large-scale energy storage systems. However, there are some challenges, involving inferior cycle stability (< 3000 cycles) and low working potential, which restrain their extensive applications. Therefore, reasonable molecular design of organics is highly required to construct high-performance zinc batteries. Herein, chalcogen atoms are introduced into the 9,10-anthraquinone (AQ) molecule, and the anthraquinone analogues with fused heteroaromatic structures are obtained with increased working potentials and energy densities. In particular, the benzo[1,2-b:4,5-b']dithiophene-4,8-dione (BDTD) is proposed as the promising cathode with a long-term lifespan of up to 12000 cycles and outstanding rate performance. Its operation mechanism involves the reversible co-coordination reaction of hydrated Zn^{2+} and H^{+} with carbonyl groups. Moreover, the good rate and cycle performance can be retained even with a high mass loading cathode (10 mg cm^{-2}), which is close to the commercial level. This work will guide the exploration of zinc-organic battery.

Introduction

In face of the worldwide energy and environment crises, developing sustainable and low-cost electrochemical energy storage systems is of great significance.[1] In the past years, lithium-ion batteries have been extensively explored, and dominated the market of digital devices and electric automobiles.[2] However, the lithium resource shortage and safety issues have increased the concern, and appropriate rechargeable battery systems should be sought to supple the growing market demand.[3] Owing to the cost effective, environmentally friendly, and sustainable nature, aqueous rechargeable batteries attract the enthusiasm of researchers and are considered as the promising candidate for grid-scale energy storage applications.[4] Among them, aqueous zinc batteries stand out because of the intrinsic advantages of zinc anode, involving suitable redox potential, high theoretical capacity of 820 mAh g^{-1}, abundant reserves and good compatibility with aqueous electrolyte.[5] Current researches focus on developing inorganic materials as the potential cathodes, such as manganese (Mn),[6] vanadium (V)-based oxide[7] and Prussian blue analogues.[8] However, these inorganic cathodes suffer from inferior cycle stability and rate performance, which are ascribed to the repeated insertion/extraction of Zn^{2+} with high charge to ionic radius ratio and sluggish ion diffusion rate in the lattice structure of the inorganic materials.[6b,9] Moreover, it is difficult for these cathodes to maintain the electrochemical performance at the commercial mass loading (10 mg cm^{-2}).[10]

Very recently, organic compounds as cathodes for aqueous zinc batteries have entered the researcher's spotlight, which possess the merit of low toxicity, high abundance, structural diversity, and high sustainability.[11] More importantly, the molecular structure of the organic compounds can be flexibly designed to adjust their electrochemical performance. Among them, the carbonyl-based organic compounds which can reversibly store monovalent and multivalent ions have been widely investigated.[12] Disappointingly, the obtained electrochemical performance of the carbonyl compounds still cannot satisfy the requirement of the practical applications, and some challenges should be solved urgently. Firstly, some of the reported carbonyl compounds exhibits excellent electrochemical performance, but with quite low discharge potential (< 0.6 V vs. Zn/Zn^{2+}). The lower working potential not only limits the energy and power densities of the batteries, but also increases the fabrication cost of battery pack for large-scale applications. According to the previous reports, introducing electron-withdrawing atoms/groups in organic compounds can decrease the lowest unoccupied molecular orbital (LUMO) energy, thereby increasing the working potential and energy density.[13] The structures of organic compounds are closely related to their electrochemical behaviors. Therefore, the reasonable molecular design strategy is highly required for carbonyl compounds, which can increase the working potential and construct the high-performance batteries. What's more, the discharged products of these carbonyl compounds generally suffer from serious instability and dissolution in aqueous electrolytes, which restrains the cycle stability of the zinc-organic batteries (about 3000 cycles). Owing to the fact that the achieved lifespan is far away from the practical application level of up to 10000 cycles,[14] using expensive ion-exchange membrane, encapsulating carbonyl compounds in the carbon

[a] Z. Li,[+] Y. Zhang,[+] J. Xu, Prof. Y. Wang
Department of Chemistry and Shanghai Key Laboratory of Molecular Catalysis and Innovative Materials, Institute of New Energy
iChEM, (Collaborative Innovation Center of Chemistry for Energy Materials)
Fudan University
Shanghai 200433, China
E-mail: ygwang@fudan.edu.cn

[+] These authors contributed equally to this work.

Supporting information for this article is available on the WWW under https://doi.org/10.1002/batt.202200431

Special Collection An invited contribution to a Special Collection on Organic Batteries.

materials, etc. are required in order to increase the cycle stability, but which will complicate the preparation processes. Although the construction of expanded organic molecules and polymerization can inhibit the dissolution of discharged products, these strategies will add units without redox activity into the organic building and decrease the theoretical capacity. Thus, finding suitable cathode materials with excellent stability is in demand for developing advanced zinc batteries. Finally, the carbonyl compounds generally display outstanding rate capacities in the aqueous electrolytes, which are achieved based on a low mass loading of the active materials in the electrode (about 3 mg cm^{-1}). However, large-scale energy storage applications put forward higher requirement on the mass loading of the electrode, and a thick electrode with a high mass loading of 10 mg cm^{-1} is required to keep cost down. And the increasing ion diffusion limitations in a thick electrode impedes the exploration of promising high mass loading cathodes.

Herein, the chalcogen atom (S or O) with electron-withdrawing property was introduced into the 9,10-anthraquinone (AQ) molecule through rational molecule design, and the electrochemical performance of the AQ, benzo[1,2-b:4,5-b']-dithiophene-4,8-dione (BDTD) and benzofuro[5,6-b]furan-4,8-dione (BFFD) cathodes were investigated in detail. Then, the promising BDTD cathode was proposed to construct the high-performance aqueous zinc-organic battery, which involves a BDTD cathode, a Zn foil anode and an aqueous 2 M $ZnSO_4$ electrolyte. The BDTD cathode exhibits the obviously increased working potential and energy/power density in comparison with the AQ cathode. The BDTD//Zn battery also performs a long-term lifespan for 12000 cycles with a high capacity retention of 81.9% and negligible self-discharge behavior due to the inherent stability of the BDTD and corresponding discharged product. Even with a high mass loading (10 mg cm^{-1}) of active materials in a thick electrode, excellent cycle stability and rate capacities can be maintained, satisfying the requirement of large-scale energy storage applications. The achieved lifespan and mass loading are much superior to the previous reports (Table S1). Moreover, in-situ attenuated total reflection-Fourier transform infrared (ATR-FTIR) analysis and cyclic voltammetry (CV) measurements were conducted to reveal the electrochemical reaction mechanism of the BDTD cathode, unveiling that the hydrated H^+ and Zn^{2+} co-coordinate reversibly with the carbonyl groups in the BDTD cathode during the discharge/charge process. Furthermore, the flexible belt-shape BDTD//Zn battery is fabricated, showing the practical application prospect in wearable and flexible electronic devices.

Results and Discussion

Recently, carbonyl compound, 9,10-anthraquinone (AQ) have been investigated as the cathode materials for aqueous zinc ion battery, which displays a high discharge capacity and excellent cycle stability.[12d,15] However, the low discharge potential of AQ cathode severely limits the energy/power density in spite of the high capacity. Introducing the electron-withdrawing atoms/groups into the organic compounds can lower the LUMO energy, which is closely associated with their reduction potential, thus a higher discharge potential can be obtained. As a proof-concept study, we selected the fused heteroaromatic molecules with built-in heteroatoms of S or O, including the benzofuro[5,6-b]furan-4,8-dione (BFFD) and benzo[1,2-b:4,5-b']dithiophene-4,8-dione (BDTD), to comprehensively investigate their electrochemical performances (Figure 1a). The electrochemical performance of the AQ, BDTD, BFFD were investigated by assembling the aqueous zinc ion batteries, involving a prepared AQ/BDTD/BFFD cathode, a Zn foil anode, and an aqueous 2 M $ZnSO_4$ electrolyte. The discharge/charge curves of the AQ//Zn, BDTD//Zn and BFFD//Zn batteries measured at 0.1 A g^{-1} were given in Figure 1(b), and the AQ cathode displays a low discharge potential of 0.53 V with a discharge capacity of 172.0 mAh g^{-1}. It can be observed obviously that the BDTD, BFFD cathodes exhibits the increased discharge potential of 0.70, 0.74 V and higher discharge capacities of 190.7, 197.3 mAh g^{-1}, respectively, indicating the significantly improved working potential compared with the AQ cathode, which is attributable to the function of the chalcogen atoms in the molecular structure. As shown in Figure 1(c), the redox peaks in the CV curves of the AQ, BDTD, BFFD cathodes increase in the order of AQ < BDTD < BFFD, which is in consistent with the discharge/charge curves, further confirming the function of the chalcogen atoms.

Owing to the obviously increased working potential, we further investigate the electrochemical performance of BDTD and BFFD electrodes in details. As the galvanostatic discharge/charge curves of the BFFD//Zn and BDTD//Zn batteries shown in Figure 2(a, b), the BFFD and BDTD cathodes display high discharge capacities of 200.8 and 206.2 mAh g^{-1} at a low current density of 0.05 A g^{-1}, respectively. Even when the current density increasing to 30 A g^{-1}, the discharge capacities of 67.0 and 64.0 mAh g^{-1} can be maintained for BFFD and BDTD electrodes. It is noteworthy that both the BFFD and BDTD cathodes perform outstanding rate properties, which are superior to the AQ cathode (Figure S1). Accordingly, the energy/power densities of the batteries were calculated based on the mass of active materials in cathode and consumed Zn anode. As the Ragone plots displayed in Figure 2(c), the AQ//Zn, BDTD//Zn, BFFD//Zn batteries exhibit the maximum energy densities of 87.2, 115.8, 121.3 Wh kg^{-1} at the power densities of 21.3, 27.9, 30.2 W kg^{-1}, and the maximum power densities of 8849.6, 13527.7, 15238.8 W kg^{-1} at the energy densities of 12.4, 28.4, 33.5 Wh kg^{-1}, respectively. It can be demonstrated that the energy/power densities of the BDTD//Zn and BFFD//Zn batteries are increased significantly in comparison with these for AQ//Zn battery. Furthermore, the cycle stability of the prepared batteries was investigated as given in Figure 2(d). At a quiet low current density of 0.1 A g^{-1}, the BFFD//Zn battery displays the fast capacity decay in the first few cycles and a capacity retention of 65.8% within 200 cycles. While the BDTD//Zn battery undergoes an active process in the first few cycles and cycles stably with a high capacity retention of 86.3%. When a high current density of 5.0 A g^{-1} was applied,

Research Article
doi.org/10.1002/batt.202200431
Chemistry Europe
European Chemical Societies Publishing

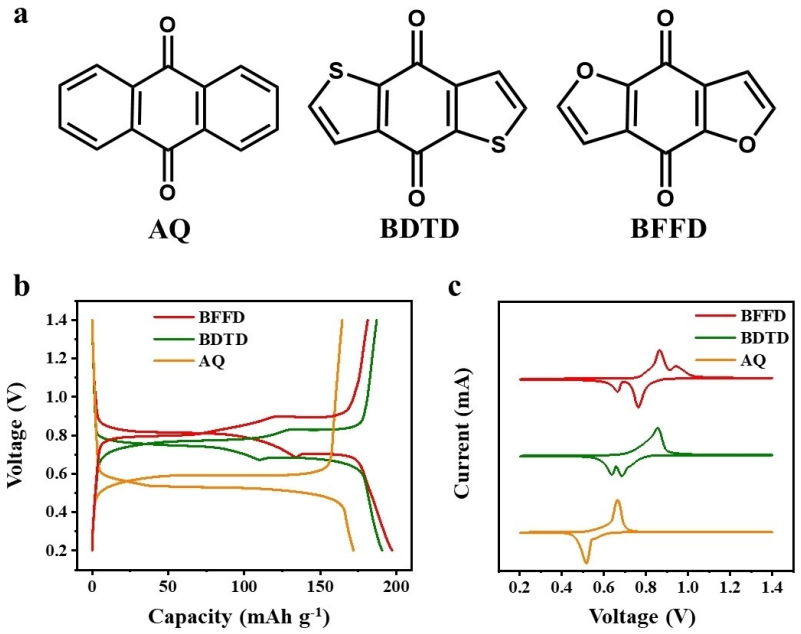

Figure 1. a) Molecular structures of the AQ, BDTD, BFFD. b) Galvanostatic discharge/charge curves of the aqueous AQ//Zn, BDTD//Zn, BFFD//Zn batteries measured at current density of 0.1 A g^{-1}. c) CV curves of the AQ//Zn, BDTD//Zn, BFFD//Zn batteries measured at a scan rate of 0.2 mV s^{-1}.

the BFFD//Zn, BDTD//Zn batteries perform the long cycle stability within 10000 and 12000 cycles with the capacity retention of 65.8% and 81.9%, respectively (Figure 2e and f). The obvious capacity decay of the BFFD//Zn battery can be observed at both low and high current densities (Figure S2). And it can be detected that the BDTD//Zn battery displays superior cycle stability compared with the BFFD//Zn and AQ//Zn batteries (Figure S3). As mentioned above, the BDTD cathode displays comparable rate property, energy/power density and outstanding cycle stability, thus the BDTD is selected as the promising cathode material for the advanced aqueous zinc ion battery. In Figure S4, the contact angles of H_2O for AQ, BDTD and BFFD films are 110°, 90° and 125°, respectively. The BDTD film has a relatively better hydrophilicity. During the initial several cycles, the electrolyte may gradually penetrate into the electrode, which may contribute to the increase in capacity.

Furthermore, the selected BDTD molecule was characterized by the transmission electron microscopy (TEM) and scanning electron microscopy (SEM), which displays a micro-cube morphology with a size of 3–5 μm (Figure S5). As the FTIR spectrum presented in Figure S6, the characteristic peaks at 1648 and 728 cm^{-1} belongs to the stretching vibration of the C=O and C–S bonds, respectively. The absorption peaks assigned to the stretching vibration of C=C bonds (1390, 1493 cm^{-1}) and bending vibration of C–H bonds (1201, 1290 cm^{-1}) can be observed clearly. The ^1H nuclear magnetic resonance (NMR) spectrum of the BDTD also certifies the high purity of the powder (Figure S7). Moreover, the redox reaction kinetics of the BDTD cathode was investigated by the CV measurements at different scan rates from 0.2 to 1 mV s^{-1} (Figure 3a) The peak current increases and the cathodic/anodic peaks shift slightly with the increasing of the scan rate. The calculated *b*-value of the three peaks according to the obtained peak currents and scan rates are 0.914, 0.971, and 0.926, demonstrating the charge storage of BDTD cathode mainly controlled by the non-diffusion process (Figure 3b). As shown in Figure S8, the capacitive contribution proportion was calculated to be 60% to 85% at scan rates of 0.2 to 1.0 mV s^{-1}. These results indicates that charge storage of BDTD electrode is predominantly controlled by the non-diffusion-controlled process and displays fast reaction kinetics. Organic small molecules/their discharged products generally suffer from serious dissolution in the aqueous electrolytes during the cycle process, displaying inferior stability. Therefore, the self-discharge/charge measurements of the BDTD//Zn battery were carried out to investigate the stability of the BDTD cathode. The battery was charged to 1.4 V, and followed by resting for 24 h. Obvious discharge platform and a discharge capacity of 166.6 mAh g^{-1} can be delivered after the rest (Figure 3c). After discharged to 0.2 V and rested for 24 h, the achieved charge capacity is approximately equal to the charge capacity (Figure 3e). During the rest process, voltage remained stable after reaching steady state (Figure 3d and f). These results indicate that there are negligible self-discharge/charge behaviors on the fully charged/discharged states, confirming the excellent stability of the BDTD as the cathode for aqueous zinc ion battery. And the dissolution of BDTD and corresponding discharged products is hardly detected, which is in accordance with the excellent cycle performance as discussed above.

Subsequently, the in-situ and ex-situ characterizations were carried out to reveal the electrochemical reaction mechanism of the BDTD cathode in aqueous 2 M $ZnSO_4$ electrolyte. X-ray photoelectron spectroscopy (XPS) measurements of the BDTD electrode at the pristine, discharged and charged states were collected. It can be detected from Figure 4(a) that the Zn 2p

Research Article
doi.org/10.1002/batt.202200431
Chemistry Europe
European Chemical Societies Publishing

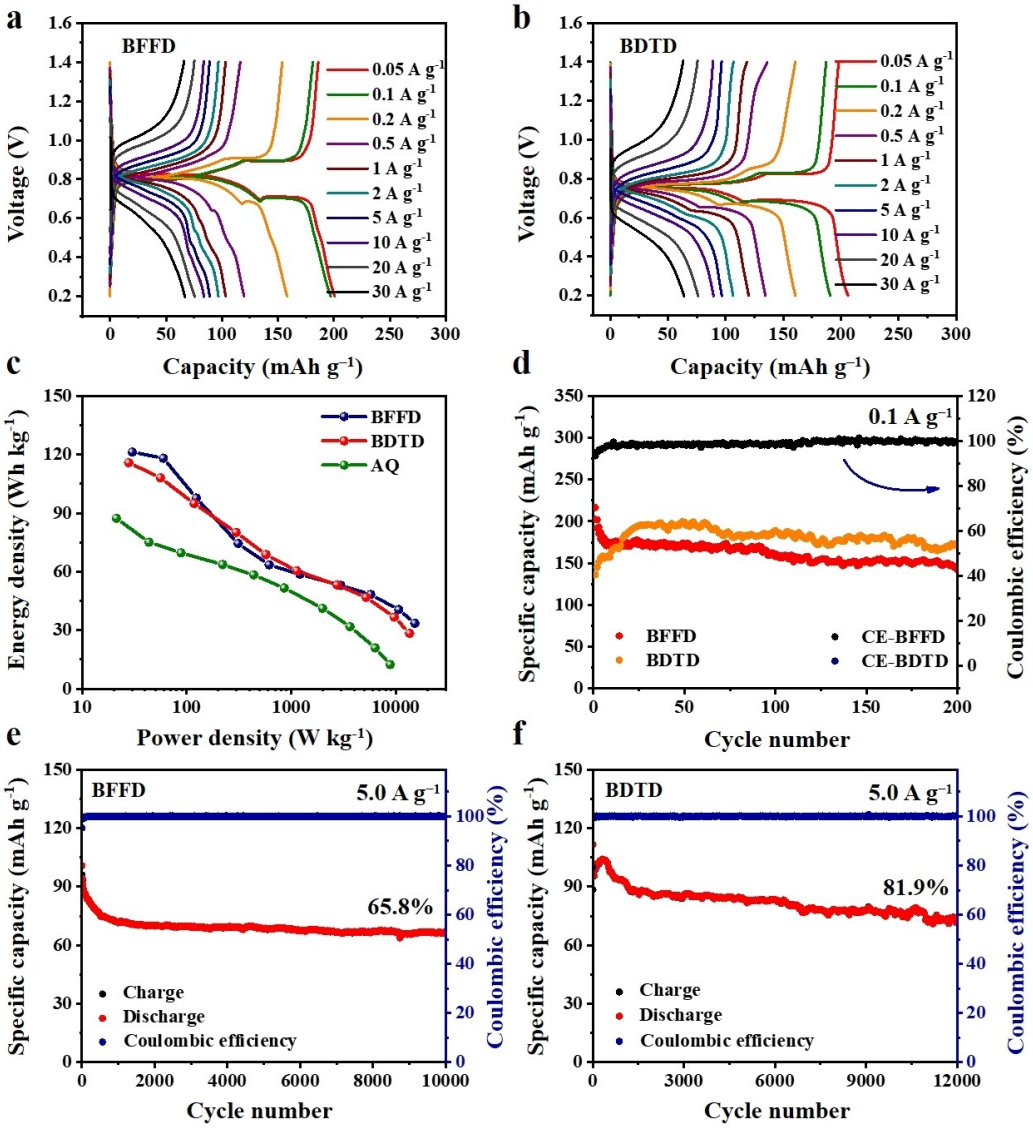

Figure 2. Electrochemical performance of the BDTD and BFFD electrodes. Rate properties of a) BFFD and b) BDTD electrode. c) Ragone plots of the BFFD//Zn, BDTD//Zn, and AQ//Zn batteries. d) Cycle stability of the BFFD//Zn and BDTD//Zn batteries at a low current density of 0.1 A g^{-1}. Cycle performance of e) BFFD//Zn and f) BDTD//Zn batteries measured at 5.0 A g^{-1}.

peaks at 1021.8 and 1044.8 eV appear in the discharged state and almost disappear after charged to 1.4 V, implying the reversible reaction of Zn^{2+} with BDTD electrode. The full survey of the XPS spectra were given in Figure S9. Moreover, owing to the fact that the hydrated H^+ with smaller size inevitably exists in the aqueous $ZnSO_4$ electrolyte, we further explore the ion co-insertion mechanism of the BDTD electrode. The CV measurements of the BDTD electrode in 2 M $ZnSO_4$ and 1 M H_2SO_4 electrolyte were carried out using the three-electrode systems. The redox peaks at −0.28, −0.32 and −0.15 V (vs. Ag/AgCl) appear in 2 M $ZnSO_4$ electrolyte, whereas redox peaks at 0.06, 0.01 and 0.13 V (vs. Ag/AgCl) appear in 1 M H_2SO_4 electrolyte (Figure 4b). The CV curves of the BDTD electrode in dilute H_2SO_4 electrolyte (the same pH value as the 2 M $ZnSO_4$ solution) can be obtained based on the Nernst equation (the detailed calculation process can be found in the Supporting information). The obtained CV curves is partially overlapped with that measured in the 2 M $ZnSO_4$ electrolyte, which demonstrates the storage of Zn^{2+} is mainly involved in the low potential region (−0.5–−0.28 V vs. Ag/AgCl), while the storage of H^+ is mainly involved in the high potential region (−0.28–−0.18 V vs. Ag/AgCl). A similar phenomenon has been reported in some recent literature.[11f,16] In order to investigate the redox center of the BDTD electrode, we conducted the in-situ ATR-FTIR test of the BDTD//Zn battery along with the CV measurement at a scan rate of 0.5 mV s^{-1}, and the FITR spectrum measured at the open-circuit state was applied as the background. According to the 2D color-filled contour plot of the in-situ ATR-FTIR spectra at different discharge/charge states (Figure 4c), the characteristic peaks at 1324 and 1443 cm^{-1} which can be assigned to the vibration of =C–O groups and C=C bonds, respectively, increase gradually during the discharge

Research Article
doi.org/10.1002/batt.202200431
Chemistry Europe
European Chemical Societies Publishing

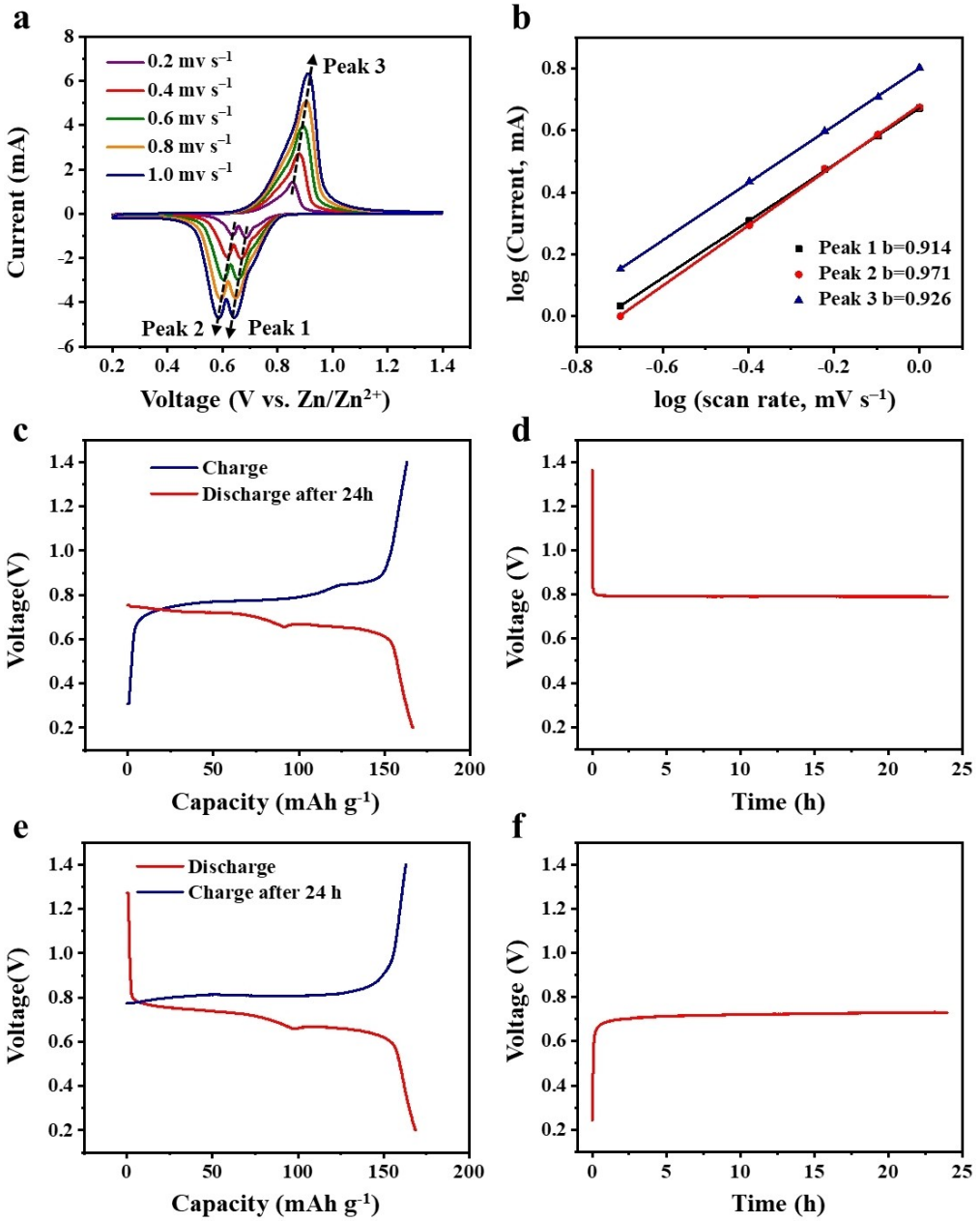

Figure 3. Reaction kinetics investigations of the BDTD electrode. a) CV curves of BDTD//Zn battery at various scan rates from 0.2 to 1 mV s^{-1}, b) log(*i*) ~ log(*v*) plots of anodic and cathodic peaks derived from the obtained CV curves. Self-discharge/charge behaviors of the BDTD//Zn battery measured at 0.2 A g^{-1}, c) when charged to 1.4 V, and then discharged to 0.2 V after rest for 24 h, d) the voltage vs. time curves at the fully charged state; e) when discharged to 0.2 V, and then charged to 1.4 V after rest for 24 h, f) the voltage vs. time curves at the fully discharged state.

process (from 1.1 to 0.2 V). This result is attributable to the binding of the carbonyl groups with the Zn^{2+} and H^+, thus the =C–O groups and C=C bonds emerge.

In the following charge process (from 0.2 to 1.4 V), the appeared characteristic peaks weaken gradually and disappear in the fully charged state. The same change trend can be observed obviously for the peaks located at 1264 cm^{-1}, which is ascribed to the stretching vibration of C–OH bonds. This result further confirms the reaction of hydrated H^+ with the carbonyl groups in BDTD, that is consistent with the above CV results. This phenomenon indicates the highly reversible coordination reaction of the C=O bonds with the cations (Zn^{2+} and H^+) in the electrolyte. Although some inorganic materials can also achieve the co-reaction of Zn^{2+} and H^+, the storage mechanism of organic materials is coordination reaction, and the storage mechanism of inorganic materials is intercalation reaction.[6c,d,16]

Because of the fast reaction kinetics of BDTD cathode and the outstanding rate performance, a thick electrode with a high mass loading (10 mg cm^{-1}) of BDTD was applied to investigate the practical applications of this battery. As shown in Figure 5(a), the high mass loading BDTD//Zn battery displays a

Research Article
doi.org/10.1002/batt.202200431
Chemistry Europe
European Chemical Societies Publishing

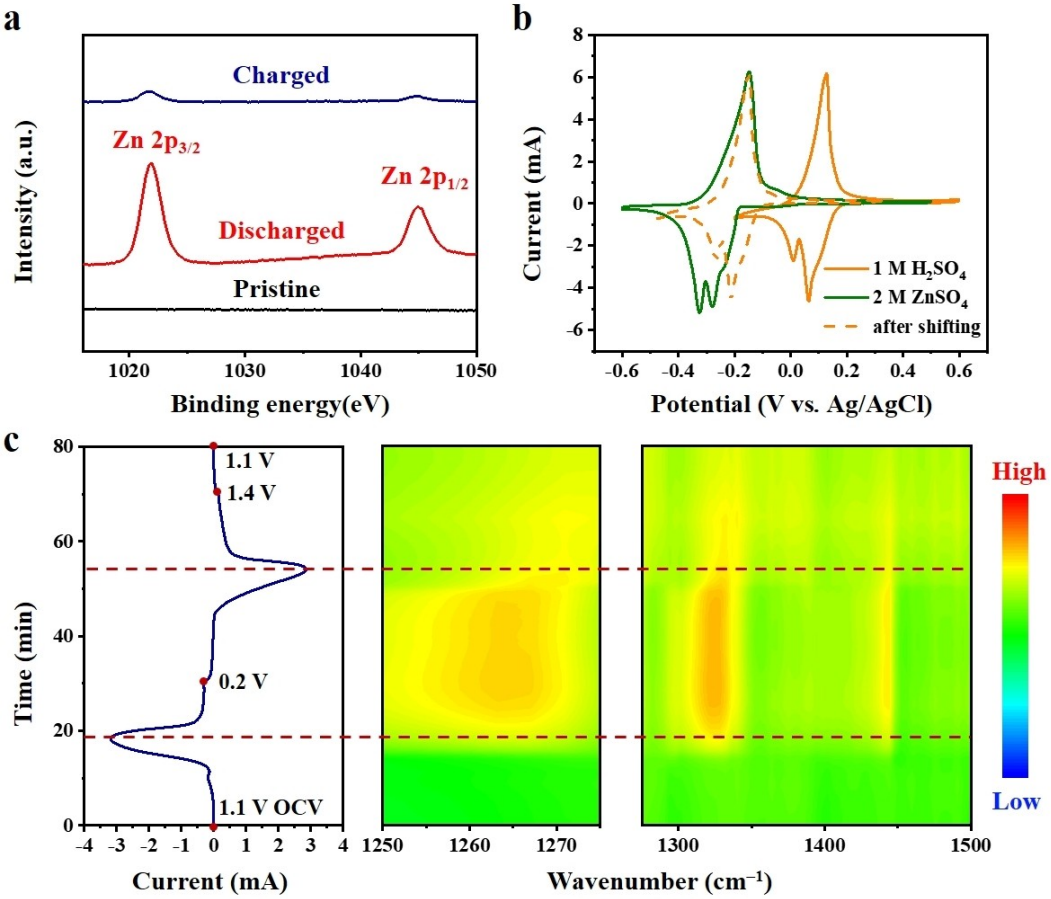

Figure 4. a) XPS spectra of Zn 2p at the pristine, discharged, and charged states. b) The CV curves of the BDTD electrode measured in 1 M H_2SO_4 and 2 M $ZnSO_4$ electrolytes, and the corresponding CV curves in dilute H_2SO_4 calculated based on the Nernst equation. c) The 2D color-filled contour plot of the in-situ ATR-FTIR spectra of the BDTD electrode during a CV test at a scan rate of 0.5 mV s^{-1} (on the left).

discharge capacity of 208 mAh g^{-1} at 0.05 A g^{-1}, which is similar to that achieved at a low mass loading of 2 mg cm^{-1}. When the current density increases to 1 A g^{-1}, a discharge capacity of 124 mAh g^{-1} can be retained, showing the decent rate performance with a capacity retention of 60%. The cycle stability of the high mass loading BDTD//Zn battery was investigated at a current density of 1 A g^{-1}. As illustrated in Figure 5b, the battery displays a long-term cycle stability of up to 700 cycles with negligible capacity fade. The achieved mass loading (10 mg cm^{-1}) of the BDTD//Zn battery is close to the commercial level, and which is superior to the recent reports (Table S1). To expand the range of practical applications, a belt-shape BDTD//Zn battery was fabricated through the vacuum sealed process. The belt-shape BDTD//Zn battery delivers almost the equal capacity at different bending angles even from 0° to 180° (Figure 5c), showing excellent flexibility. Moreover, one such belt-shape BDTD//Zn battery can power an electric fan energetically at flat, bended 90° and 180° states (Figure 5d), demonstrating the application prospects in wearable electronic devices.

Conclusion

In summary, the chalcogen atoms (O and S) were introduced into the AQ molecule to obtain the BDTD and BFFD molecules through rational molecule design. The electrochemical behaviors of the AQ, BDTD and BFFD cathode were investigated in detail, demonstrating that the obviously increased working potential and energy/power densities can be obtained in the BDTD and BFFD cathodes. Furthermore, the BDTD cathode with excellent rate property of up to 30 A g^{-1} and long-term cycle stability of up to 12000 cycles was selected as the promising cathode for constructing high-performance aqueous zinc-organic battery. The BDTD cathode also displays negligible self-discharge/charge behaviors due to the intrinsic stability of the BDTD and corresponding discharged products. Moreover, the BDTD cathode undergoes the hydrated H^+ and Zn^{2+} co-coordination reaction with the carbonyl groups in the BDTD molecules during the discharge/charge process, which is verified by the in-situ ATR-FITR tests and electrochemical measurements. Furthermore, considering the practical applications, a thick electrode with a high mass loading of 10 mg cm^{-1} was prepared, and decent electrochemical performance can be retained, showing the application prospects. A flexible belt-

Research Article
doi.org/10.1002/batt.202200431
Chemistry Europe
European Chemical Societies Publishing

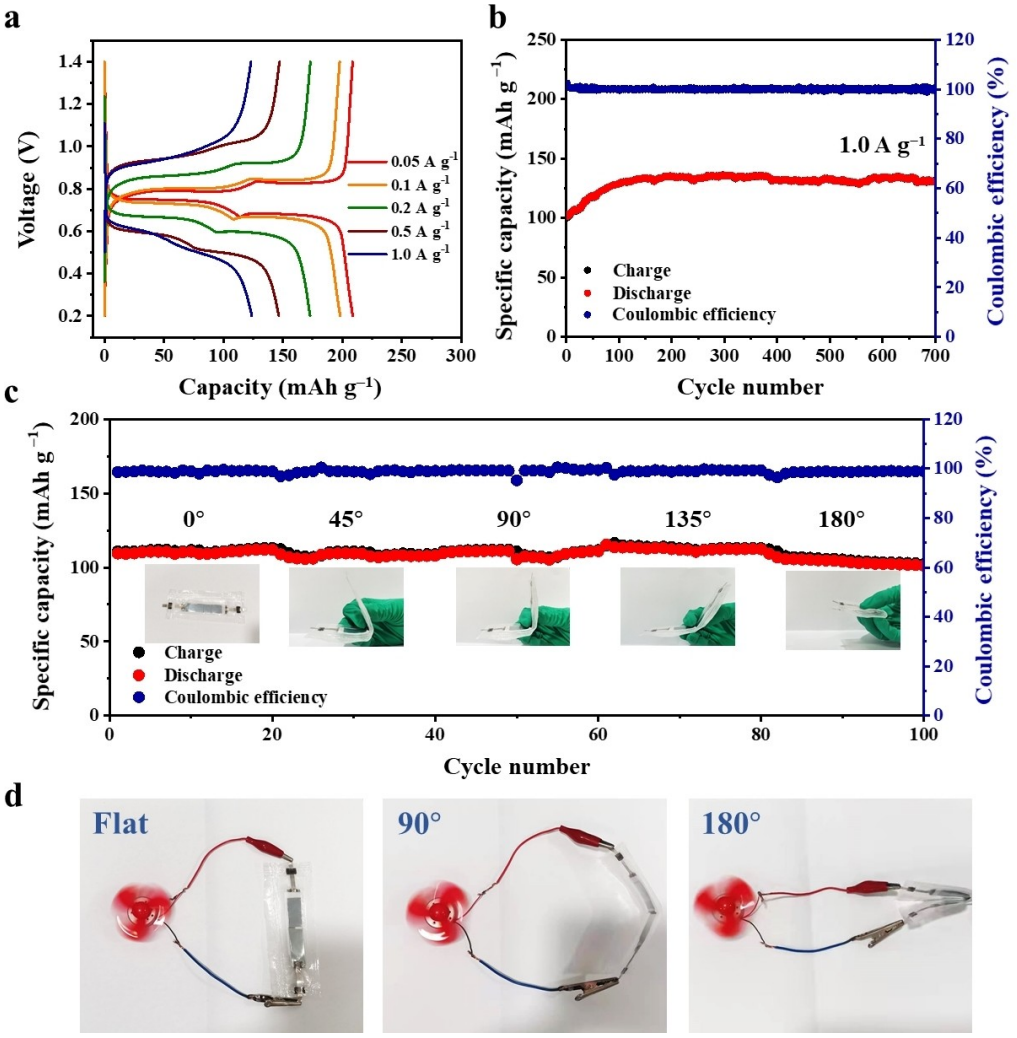

Figure 5. a) Rate properties of the high mass loaded BDTD//Zn battery. b) Cycle performance of the high mass loaded BDTD//Zn battery. c) Cycle stability of the belt-shape BDTD//Zn battery at various bending angels from 0° to 180°. d) Optical images of motivating an electric fan using a belt-shape battery at various bending angels.

shape BDTD//Zn battery is also fabricated and displays excellent flexibility. This work will guide the design of organic electrodes for aqueous zinc batteries through the relationship between molecular structure and electrochemical performance, and also shed light on expanding the application range of zinc batteries.

Experimental Section

Electrode preparation

AQ, BDTD, BFFD powders were purchased from Aladdin and used without further purification. The powders were mixed with conductive additive (Ketjen black) and binder (polytetrafluorethylene (PTFE), 60 wt.% dispersion in H_2O) with a weight ratio of 6:3:1 in the isopropanol solvent. The above slurry was rolled into a film and dried at 80 °C for 12 h. Then, the AQ, BDTD, BFFD electrodes were prepared by compressing the film on the titanium mesh current collector with a mass loading of about 3 mg cm^{-2}.

Material characterization

The material was characterized by the SEM (JEOL JSM-6390), TEM (Tecnai G2 F20 S-Twin), FTIR (Thermo Fisher Nicolet 6700 FTIR spectrometer), 1H-NMR (500 MHz, DMSO). The in-situ ATR-FTIR spectra were measured using Thermo Fisher Nicolet 6700 FTIR spectrometer with an attenuated total reflection sample cell. The ex-situ XPS spectra of the BDTD electrode were acquired using PHI 5000 C&PHI5300 X-ray photoelectron spectrometer.

Electrochemical tests

The coin cells (CR2016 type) were fabricated with the prepared electrode as cathode, Zn foil as anode, 2 M $ZnSO_4$ as the aqueous electrolyte, and glass fiber as the separator. For the three-electrode systems, the prepared BDTD electrode, active carbon and Ag/AgCl were used as working electrode, counter electrode and reference, respectively. The belt-shape BDTD//Zn battery was assembled with a BDTD cathode (1 cm×5 cm), a Zn foil anode (1 cm×5 cm) and a Whatman glass fiber separator wetted by electrolyte through a vacuum sealed process. The galvanostatic discharge/charge measurements were performed by the Hukuto Denko battery system (HJ

Research Article
doi.org/10.1002/batt.202200431

series). The self-discharge/charge behaviors of the BDTD//Zn battery were performed on a Land CT2001A battery test system (Wuhan). The CV measurements at different scan rates were conducted on the Bio-Logic electrochemical workstation. The calculated CV curves of the BDTD electrode in dilute H_2SO_4 electrolyte were obtained based on the Nernst equation.

Calculation based on Nernst Equation

Electrode reaction:

$$\mathrm{BDTD} + n\mathrm{H}^+ + ne^- \rightleftharpoons \mathrm{H}_n\mathrm{BDTD}$$

Nernst equation:

$$\varphi = \varphi^\theta + \frac{2.303RT}{nF}\lg\frac{[\mathrm{BDTD}][\mathrm{H}^+]^n}{[\mathrm{H}_n\mathrm{BDTD}]} = \varphi^\theta + \frac{0.0592}{n}\lg\frac{[\mathrm{BDTD}][\mathrm{H}^+]^n}{[\mathrm{H}_n\mathrm{BDTD}]}$$

where φ is the electrode potential; φ^θ is the standard potential; R is the universe gas constant, 8.314 $\mathrm{J\,K^{-1}\,mol^{-1}}$; T is the temperature, 298.15 K; n is the electrode transfer number; F is the Faraday constant, 96485 $\mathrm{C\,mol^{-1}}$. The activity of solid BDTD and H_nBDTD is considered as 1, then the equation can be simplified as:

$$\varphi = \varphi^\theta + \frac{0.0592}{n}\lg[\mathrm{H}^+]^n = \varphi^\theta + 0.0592\lg[\mathrm{H}^+]$$

Thus, the potential difference of the BDTD electrode in 1 M H_2SO_4 and dilute H_2SO_4 (pH ~5) can be calculated, and the CV curves of the BDTD electrode in dilute electrolyte can be obtained as shown in Figure 4(b).

Acknowledgements

The authors acknowledge the funding support from the National Natural Science Foundation of China (21975052) and the State Key Basic Research Program of China (2018YFE0201702).

Conflict of Interest

The authors declare no conflict of interest.

Data Availability Statement

The data that support the findings of this study are available from the corresponding author upon reasonable request.

[1] a) B. Dunn, H. Kamath, J. M. Tarascon, *Science* **2011**, *334*, 928–935; b) L. E. Blanc, D. Kundu, L. F. Nazar, *Joule* **2020**, *4*, 771–799.
[2] J. B. Goodenough, K. S. Park, *J. Am. Chem. Soc.* **2013**, *135*, 1167–1176.
[3] L. Ma, M. A. Schroeder, O. Borodin, T. P. Pollard, M. S. Ding, C. S. Wang, K. Xu, *Nat. Energy* **2020**, *5*, 743–749.
[4] a) J. Y. Luo, W. J. Cui, P. He, Y. Y. Xia, *Nat. Chem.* **2010**, *2*, 760–765; b) W. Chen, G. D. Li, A. Pei, Y. Z. Li, L. Liao, H. X. Wang, J. Y. Wan, Z. Liang, G. X. Chen, H. Zhang, J. Y. Wang, Y. Cui, *Nat. Energy* **2018**, *3*, 428–435; c) X. L. Dong, L. Chen, J. Y. Liu, S. Haller, Y. G. Wang, Y. Y. Xia, *Sci. Adv.* **2016**, *2*, e1501038; d) M. Li, Z. L. Li, X. P. Wang, J. S. Meng, X. Liu, B. K. Wu, C. H. Han, L. Q. Mai, *Energy Environ. Sci.* **2021**, *14*, 3796–3839; e) H. J. Yang, Y. Qiao, Z. Chang, H. Deng, P. He, H. S. Zhou, *Adv. Mater.* **2020**, *32*, 2004240; f) X. Y. Wu, Y. T. Qi, J. J. Hong, Z. F. Li, A. S. Hernandez, X. L. Ji, *Angew. Chem. Int. Ed.* **2017**, *56*, 13026–13030; *Angew. Chem.* **2017**, *129*, 13206–13210; g) L. W. Jiang, Y. X. Lu, C. L. Zhao, L. L. Liu, J. N. Zhang, Q. Q. Zhang, X. Shen, J. M. Zhao, X. Q. Yu, H. Li, X. J. Huang, L. Q. Chen, Y. S. Hu, *Nat. Energy* **2019**, *4*, 495–503; h) Y. Zhang, L. Zhao, Y. Liang, X. Wang, Y. Yao, *eScience* **2022**, *2*, 110–115; i) Z. Wang, M. Zhou, L. Qin, M. Chen, Z. Chen, S. Guo, L. Wang, G. Fang, S. Liang, *eScience* **2022**, *2*, 209–218.
[5] a) Y. Zhao, Y. X. Huang, F. Wu, R. J. Chen, L. Li, *Adv. Mater.* **2021**, *33*, 2106469; b) D. L. Chao, C. Ye, F. X. Xie, W. H. Zhou, Q. H. Zhang, Q. F. Gu, K. Davey, L. Gu, S. Z. Qiao, *Adv. Mater.* **2020**, *32*, 2001894; c) Z. X. Liu, Q. Yang, D. H. Wang, G. J. Liang, Y. H. Zhu, F. N. Mo, Z. D. Huang, X. L. Li, L. T. Ma, T. C. Tang, Z. G. Lu, C. Y. Zhi, *Adv. Energy Mater.* **2019**, *9*, 1902473; d) Z. Wang, J. H. Huang, Z. W. Guo, X. L. Dong, Y. Liu, Y. G. Wang, Y. Y. Xia, *Joule* **2019**, *3*, 1289–1300; e) L. T. Kang, M. W. Cui, Z. T. Zhang, F. Y. Jiang, *Batteries & Supercaps* **2020**, *3*, 966–1005; f) B. Y. Tang, L. T. Shan, S. Q. Liang, J. Zhou, *Energy Environ. Sci.* **2019**, *12*, 3288–3304.
[6] a) H. L. Pan, Y. Y. Shao, P. F. Yan, Y. W. Cheng, K. S. Han, Z. M. Nie, C. M. Wang, J. H. Yang, X. L. Li, P. Bhattacharya, K. T. Mueller, J. Liu, *Nat. Energy* **2016**, *1*, 16039; b) J. H. Huang, Z. Wang, M. Y. Hou, X. L. Dong, Y. Liu, Y. G. Wang, Y. Y. Xia, *Nat. Commun.* **2018**, *9*, 2906; c) Y. X. Liao, H. C. Chen, C. Yang, R. Liu, Z. W. Peng, H. J. Cao, K. K. Wang, *Energy Storage Mater.* **2022**, *44*, 508–516; d) Y. Ma, M. Xu, R. Liu, H. H. Xiao, Y. Liu, X. Wang, Y. Y. Huang, G. H. Yuan, *Energy Storage Mater.* **2022**, *48*, 212–222.
[7] a) D. Kundu, B. D. Adams, V. Duffort, S. H. Vajargah, L. F. Nazar, *Nat. Energy* **2016**, *1*, 16119; b) F. Wan, Z. Q. Niu, *Angew. Chem. Int. Ed.* **2019**, *58*, 16358–16367; *Angew. Chem.* **2019**, *131*, 16508–16517; c) F. W. Ming, H. F. Liang, Y. J. Lei, S. Kandambeth, M. Eddaoudi, H. N. Alshareef, *ACS Energy Lett.* **2021**, *6*, 2982–2982.
[8] a) L. Y. Zhang, L. Chen, X. F. Zhou, Z. P. Liu, *Adv. Energy Mater.* **2015**, *5*, 1400930; b) Y. X. Zeng, X. F. Lu, S. L. Zhang, D. Y. Luan, S. Li, X. W. Lou, *Angew. Chem. Int. Ed.* **2021**, *60*, 22189–22194; *Angew. Chem.* **2021**, *133*, 22363–22368.
[9] T. Sun, Z. J. Li, Y. F. Zhi, Y. J. Huang, H. J. Fan, Q. C. Zhang, *Adv. Funct. Mater.* **2021**, *31*, 2010049.
[10] a) H. T. Sun, L. Mei, J. F. Liang, Z. P. Zhao, C. Lee, H. L. Fei, M. N. Ding, J. Lau, M. F. Li, C. Wang, X. Xu, G. L. Hao, B. Papandrea, I. Shakir, B. Dunn, Y. Huang, X. F. Duan, *Science* **2017**, *356*, 599–604; b) H. Z. Zhang, Y. B. Fang, F. Yang, X. Q. Liu, X. H. Lu, *Energy Environ. Sci.* **2020**, *13*, 2515–2523.
[11] a) T. B. Schon, B. T. McAllister, P. F. Li, D. S. Seferos, *Chem. Soc. Rev.* **2016**, *45*, 6345–6404; b) Y. Lu, J. Chen, *Nat. Chem. Rev.* **2020**, *4*, 127–142; c) J. Xie, Q. C. Zhang, *Small* **2019**, *15*, 1805061; d) Z. W. Tie, Z. Q. Niu, *Angew. Chem. Int. Ed.* **2020**, *59*, 21293–21303; *Angew. Chem.* **2020**, *132*, 21477–21487; e) D. Kundu, P. Oberholzer, C. Glaros, A. Bouzid, E. Tervoort, A. Pasquarello, M. Niederberger, *Chem. Mater.* **2018**, *30*, 3874–3881; f) Z. W. Tie, L. J. Liu, S. Z. Deng, D. B. Zhao, Z. Q. Niu, *Angew. Chem. Int. Ed.* **2020**, *59*, 4920–4924; *Angew. Chem.* **2020**, *132*, 4950–4954; g) L. Yan, Y. Zhang, Z. G. Ni, Y. Zhang, J. Xu, T. Y. Kong, J. H. Huang, W. Li, J. Ma, Y. G. Wang, *J. Am. Chem. Soc.* **2021**, *143*, 15369–15377; h) M. A. Khayum, M. Ghosh, V. Vijayakumar, A. Halder, M. Nurhuda, S. Kumar, M. Addicoat, S. Kurungot, R. Banerjee, *Chem. Sci.* **2019**, *10*, 8889–8894; i) B. Haupler, C. Rossel, A. M. Schwenke, J. Winsberg, D. Schmidt, A. Wild, U. S. Schubert, *NPG Asia Mater.* **2016**, *8*, e283; j) H. Glatz, E. Lizundia, F. Pacifico, D. Kundu, *ACS Appl. Energ. Mater.* **2019**, *2*, 1288–1294.
[12] a) Z. W. Guo, J. H. Huang, X. L. Dong, Y. Y. Xia, L. Yan, Z. Wang, Y. G. Wang, *Nat. Commun.* **2020**, *11*, 959; b) J. H. Huang, X. L. Dong, Z. W. Guo, Y. G. Wang, *Angew. Chem. Int. Ed.* **2020**, *59*, 18322–18333; *Angew. Chem.* **2020**, *132*, 18478–18489; c) Y. L. Liang, Y. Jing, S. Gheytani, K. Y. Lee, P. Liu, A. Facchetti, Y. Yao, *Nat. Mater.* **2017**, *16*, 841–848; d) Q. Zhao, W. W. Huang, Z. Q. Luo, L. J. Liu, Y. Lu, Y. X. Li, L. Li, J. Y. Hu, H. Ma, J. Chen, *Sci. Adv.* **2018**, *4*, 10, eaao1761; e) Z. W. Guo, Y. Y. Ma, X. L. Dong, J. H. Huang, Y. G. Wang, Y. Y. Xia, *Angew. Chem. Int. Ed.* **2018**, *57*, 11737–11741; *Angew. Chem.* **2018**, *130*, 11911–11915; f) J. Xie, F. Yu, J. W. Zhao, W. Guo, H. L. Zhang, G. L. Cui, Q. C. Zhang, *Energy Storage Mater.* **2020**, *33*, 283–289; g) H. Y. Shi, Y. J. Ye, K. Liu, Y. Song, X. Q. Sun, *Angew. Chem. Int. Ed.* **2018**, *57*, 16359–16363; *Angew. Chem.* **2018**, *130*, 16597–16601; h) G. Dawut, Y. Lu, L. C. Miao, J. Chen, *Inorg. Chem. Front.* **2018**, *5*, 1391–1396; i) C. P. Han, H. F. Li, Y. Li, J. X. Zhu, C. Y. Zhi, *Nat. Commun.* **2021**, *12*, 2400; j) F. Wang, X. L. Fan, T. Gao, W. Sun, Z. H. Ma, C. Y. Yang, F. Han, K. Xu, C. S. Wang, *ACS Cent. Sci.* **2017**, *3*, 1121–1128.
[13] a) Y. L. Liang, P. Zhang, J. Chen, *Chem. Sci.* **2013**, *4*, 1330–1337; b) Z. L. Ye, S. J. Xie, Z. Y. Cao, L. P. Wang, D. X. Xu, H. Zhang, J. Matz, P. Dong,

H. Y. Fang, J. F. Shen, M. X. Ye, *Energy Storage Mater.* **2021**, *37*, 378–386; c) D. Y. Shen, A. M. Rao, J. Zhou, B. A. Lu, *Angew. Chem. Int. Ed.* **2022**, *61*, e202201972; *Angew. Chem.* **2022**, *134*, e202201972; d) H. L. Cui, T. R. Wang, Z. D. Huang, G. J. Liang, Z. Chen, A. Chen, D. H. Wang, Q. Yang, H. Hong, J. Fan, C. Y. Zhi, *Angew. Chem. Int. Ed.* **2022**, *61*, e202203453; *Angew. Chem.* **2022**, *134*, e202203453.

[14] G. L. Soloveichik, *Nature* **2014**, *505*, 163–165.

[15] L. J. Yan, X. M. Zeng, Z. H. Li, X. J. Meng, D. Wei, T. F. Liu, M. Ling, Z. Lin, C. D. Liang, *Mater. Today Energy* **2019**, *13*, 323–330.

[16] Y. R. Wang, C. X. Wang, Z. G. Ni, Y. M. Gu, B. L. Wang, Z. W. Guo, Z. Wang, D. Bin, J. Ma, Y. G. Wang, *Adv. Mater.* **2020**, *32*, 2000338.

Manuscript received: September 29, 2022
Revised manuscript received: November 6, 2022
Accepted manuscript online: November 10, 2022
Version of record online: November 30, 2022